

A 1.1- / 0.9-nA Temperature-Independent 213- / 565-ppm/°C Self-Biased CMOS-Only Current Reference in 65-nm Bulk and 22-nm FDSOI

Martin Lefebvre, *Graduate Student Member, IEEE*, Denis Flandre, *Senior Member, IEEE*, and David Bol, *Senior Member, IEEE*

Abstract—In many applications, the ability of current references to cope with process, voltage and temperature (PVT) variations is critical to maintain system-level performance. However, temperature-independent current references operating in the nA range are rarely area-efficient due to the use of large resistors which occupy a significant silicon area at this current level. In this paper, we introduce a nA-range constant-with-temperature (CWT) current reference relying on a self-cascode MOSFET (SCM), biased by a proportional-to-absolute-temperature voltage with a CWT offset. On the one hand, the proposed reference has been simulated post-layout in 65-nm bulk. This design consumes 5.4 nW at 0.7 V and achieves a 1.1-nA current with a line sensitivity (LS) of 0.69 %/V and a temperature coefficient (TC) of 213 ppm/°C. On the other hand, the proposed reference has been simulated and fabricated in 22-nm fully-depleted silicon-on-insulator (FDSOI). This second design requires additional features to mitigate the impact of parasitic diode leakage at high temperature. In measurement, it consumes 5.8 nW at 0.9 V and achieves a 0.9-nA current with a 0.39-%/V LS and a 565-ppm/°C TC. As a result of using an SCM, the proposed references occupy a silicon area of 0.0021 mm² in 65 nm (resp. 0.0132 mm² in 22 nm) at least 25× (resp. 4×) smaller than state-of-the-art CWT references operating in the same current range.

Index Terms—Current reference, temperature coefficient (TC), temperature-independent, constant-with-temperature (CWT), self-cascode MOSFET (SCM).

I. INTRODUCTION

DESIGNING current references to bias analog blocks constituting Internet-of-Things (IoT) nodes, such as low-power operational amplifiers [1] and wake-up timers [2], requires these references to be both area-efficient and robust to process, voltage and temperature (PVT) variations. This task appears to be of particular difficulty in the nA range, with Fig. 1(a) highlighting the absence of area-efficient solutions for the generation of a constant-with-temperature (CWT) nA-range current. This gap originates from the fact that conventional CWT current references [Fig. 1(b)] consist in applying a reference voltage to a voltage-to-current converter, which is usually implemented by a gate-leakage transistor [3], [4], [5] or a resistor [6], [7]. These converters are well suited to the generation of a pA- or μ A-range current, in the sense

This work was supported by the Fonds de la Recherche Scientifique (FRS-FNRS) of Belgium under grant CDR J.0014.20. (Corresponding author: Martin Lefebvre.) The authors are with the ICTEAM Institute, Université catholique de Louvain (UCLouvain), 1348 Louvain-la-Neuve, Belgium (e-mail: {martin.lefebvre; denis.flandre; david.bol}@uclouvain.be). Color versions of one or more figures in this article are available at <https://doi.org/10.1109/JSSC.2023.3240209>. Digital Object Identifier 10.1109/JSSC.2023.3240209

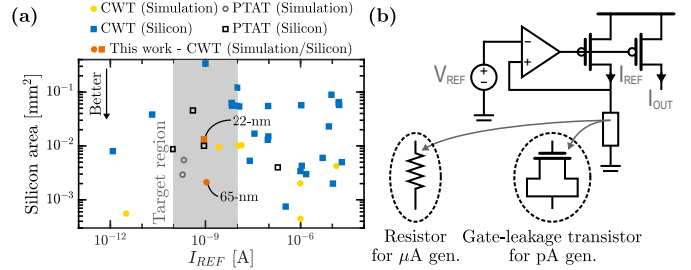


Fig. 1. (a) Trade-off between silicon area and reference current, based on prior art, highlighting the absence of area-efficient solutions for the generation of a nA-range CWT current. (b) Conventional CWT current references are based on a reference voltage applied to a gate-leakage transistor or a resistor, which are respectively well suited to the generation of a pA- or μ A-range current.

that they occupy a reasonable silicon area at this current level. Unfortunately, the generation of a nA-range current would lead to a much larger area, as the resistance of the gate-leakage transistor (resp. resistor) needs to be decreased (resp. increased) by placing devices in parallel (resp. series). Besides, proportional-to-absolute-temperature (PTAT) current references operating in the nA range, such as [8], [9], are area-efficient because they rely on a self-cascode MOSFET (SCM) biased with a PTAT voltage. This structure generates a current proportional to the so-called specific sheet current and thus, to temperature. Even though prior designs have tried to harness the area efficiency of SCMs to generate a CWT current [10], [11], they cannot easily be ported to other technologies as they rely on a particular temperature dependence of the specific sheet current. An even more important challenge is thus to tackle key criteria such as the temperature coefficient (TC) and line sensitivity (LS) in the specific case of current references operating in the nA range.

In this work, we propose a nA-range CWT current reference based on an SCM, which differs from [8], [9] by the addition of a CWT offset to the PTAT voltage biasing the SCM. This offset voltage is key in making SCM-based references CWT, and is obtained as the threshold voltage difference ΔV_T between two transistors of the same V_T type, one of them being forward body-biased to reduce its threshold voltage. For the sake of generalization, this work expands on our conference paper [12] by demonstrating the feasibility of the proposed reference in a conventional bulk technology, compared to fully-depleted silicon-on-insulator (FDSOI) only in [12]. The proposed reference is validated in two CMOS technologies through post-layout simulations in TSMC 65-nm bulk and measurements in GlobalFoundries (GF) 22-nm FDSOI. In addition, it provides additional insight into the design, archi-

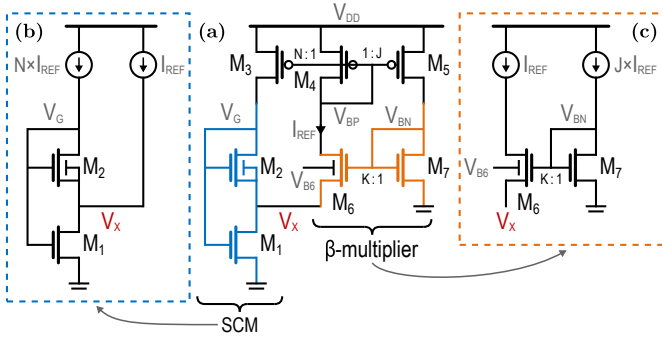


Fig. 2. Basic schematic of the proposed current reference, which consists of an SCM formed by M_{1-2} (in blue) and further simplified in (b), and a β -multiplier composed of M_{6-7} (in orange) summarized in (c).

texture and post-layout simulations of the reference in both technologies. The paper is structured as follows. Section II explains the operation principle of the proposed reference based on its governing equations. Next, Section III details the methodology used to size the reference. Then, Section IV discusses design optimizations, as well as simulation results in 65 and 22 nm, while Section V presents the measurement results in 22 nm. Finally, Section VI compares the proposed reference to the state of the art, and Section VII offers some concluding remarks.

II. GOVERNING EQUATIONS AND OPERATION PRINCIPLE

In this section, our first objective is to explain how the addition of a CWT offset to the voltage biasing the SCM leads to a temperature-independent reference current, based on general equations governing the current reference behavior. Then, we highlight the differences with respect to PTAT references [8], [9] and detail how temperature independence is achieved in the proposed reference with generic parameters. Finally, we compare different ways of implementing the offset voltage.

A. Governing Equations

To establish the equations governing the reference, we rely on the schematic in Fig. 2(a), which consists of two main elements: an SCM and a β -multiplier, both supplied by pMOS current mirrors. First, the SCM relies on long-channel transistors in moderate inversion, for which a simplified model such as the analog compact MOSFET (ACM) model [13] is adequate to describe the transistor current-voltage (I-V) curve. In this model, the drain current is given by

$$I_D = I_{SQ} S (i_f - i_r), \quad (1)$$

where $I_{SQ} = \frac{1}{2} \mu C'_{ox} n U_T^2$ is the specific sheet current, μ is the carrier mobility, C'_{ox} is the normalized gate oxide capacitance, n is the subthreshold slope factor, U_T is the thermal voltage, $S = W/L$ is the transistor aspect ratio, and i_f , i_r are the forward and reverse inversion levels. The transistor I-V curve is captured by

$$V_P - V_S = U_T \left[\sqrt{1 + i_f} - 2 + \log \left(\sqrt{1 + i_f} - 1 \right) \right], \quad (2)$$

where $V_P = (V_G - V_{T0})/n$ is the pinch-off voltage, V_{T0} is the threshold voltage at zero V_{BS} , and all voltages are referred to the transistor's body. A similar equation is obtained for the reverse inversion level, by replacing i_f by i_r and V_S by V_D in

(2), but it is only relevant when the transistor is not saturated.

Two distinct expressions of voltage V_X are obtained by applying the ACM equations to transistors M_{1-2} forming the SCM, and are given by (24) and (25) in Appendix A with $\alpha \triangleq i_{f1}/i_{f2} > 1$ and $\beta \triangleq i_{r1}/i_{f2} \in [0; 1]$. Then, the ratio of the aspect ratios of M_{1-2} must comply with

$$\frac{S_1}{S_2} = \frac{I_{SQ2}}{I_{SQ1}} \frac{1+N}{N} \frac{1}{\alpha - \beta} \quad (3)$$

to ensure that Kirchhoff's current law is respected, N being the current ratio between M_3 and M_4 . Next, the ACM equations are applied to the weak-inversion transistors M_{6-7} constituting the β -multiplier [Fig. 2(c)]. We consider two distinct cases to obtain the expression of voltage V_X . First, the case in which $V_{B6} = V_X$ and M_{6-7} have different threshold voltages. In this case, V_X is given by

$$V_X \simeq n_6 U_T \log(JK) + \left(\frac{n_6}{n_7} V_{T07} - V_{T06} \right), \quad (4)$$

$$= n U_T \log(JK) + (V_{T07} - V_{T06}), \quad (5)$$

J and K being current mirror ratios, with (4) corresponding to transistors with different V_T types and hence entirely distinct characteristics, and (5) to transistors of the same V_T type but with different lengths, and thus similar characteristics except for their V_{T0} . Second, we deal with the case in which $V_{B6} > V_X$, M_{6-7} have the same V_T type and length, and forward body / back-gate biasing (FBB) is leveraged to reduce V_{T6} . If the impact of the body effect on threshold voltage is modeled as $V_T = V_{T0} - \gamma_b V_{BS}$ for an nMOS, with γ_b denoting the body factor, voltage V_X is computed as

$$V_X = n U_T \log(JK) + \gamma_b (V_{B6} - V_X). \quad (6)$$

Ultimately, regardless of the origin of ΔV_T , (4) to (6) boil down to a single expression

$$V_X = n U_T \log(K_{PTAT}) + \Delta V_T, \quad (7)$$

with $K_{PTAT} \triangleq JK$. Connecting the SCM and the β -multiplier as in Fig. 2(a) amounts to equating (24) and (7), and leads to

$$\left[\left(\sqrt{1 + \alpha i_{f2}} - \sqrt{1 + i_{f2}} \right) + \log \left(\frac{\sqrt{1 + \alpha i_{f2}} - 1}{\sqrt{1 + i_{f2}} - 1} \right) \right] \\ = \log(K_{PTAT}) + \frac{\Delta V_T}{n U_T}, \quad (8)$$

in which only the term highlighted in red is temperature-dependent due to the combined temperature dependence of ΔV_T and U_T . Besides, applying (1) to M_2 gives the expression of the reference current

$$I_{REF}(T) = I_{SQ2}(T) i_{f2}(T) (S_2/N), \quad (9)$$

where $I_{SQ2}(T) \propto U_T^2 \mu(T) \propto T^{2-m}$, with $\mu(T) = \mu(T_0) (T/T_0)^{-m}$, and m is the temperature exponent of the carrier mobility. An important quantity which remains to be defined is the sensitivity of the reference current to V_X ,

$$S_{I_{REF}} = \frac{1}{I_{REF}} \frac{dI_{REF}}{dV_X} = \frac{1}{I_{REF}} \frac{dI_{REF}}{di_{f2}} \frac{di_{f2}}{dV_X}, \quad (10)$$

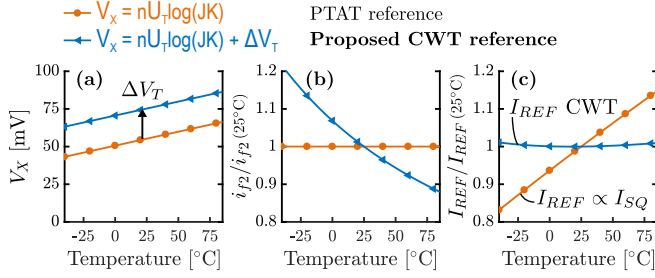


Fig. 3. Operation principle of PTAT references proposed in prior art [8], [9] (in orange) and of the proposed CWT reference (in blue). Analytical expression of (a) the voltage V_X applied to the SCM, (b) the inversion level of M_2 , denoted as i_{f2} , and (c) the reference current I_{REF} , as a function of temperature and for $\Delta V_T = 20$ mV. Generic technological parameters $n = 1.2$ and $m = 1.25$ are selected. (b) and (c) are normalized by their value at 25°C . For the proposed CWT reference, the parameters leading to a minimum I_{REF} TC are $K_{PTAT} = 6$ and $\alpha = 2.9$.

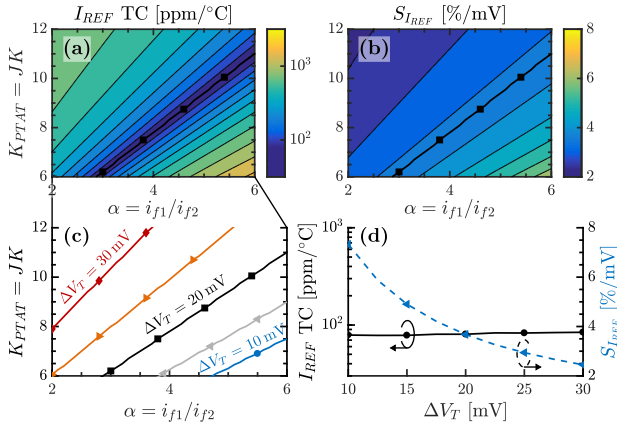


Fig. 4. Analytical expression for (a) the TC of I_{REF} and (b) the sensitivity $S_{I_{REF}}$, as a function of K_{PTAT} and α , and for the same technological parameters as Fig. 3. (c) Location of the I_{REF} TC valley in the $(K_{PTAT}; \alpha)$ space, for ΔV_T ranging from 10 to 30 mV. (d) I_{REF} TC and $S_{I_{REF}}$ as a function of ΔV_T , for $\alpha = 4$ and the optimal value of K_{PTAT} .

with I_{REF} expressed by (9) and di_{f2}/dV_X computed from (24), consequently yielding

$$S_{I_{REF}} = \frac{2}{i_{f2}n_2U_T} \left[\frac{\alpha}{\sqrt{1 + \alpha i_{f2}} - 1} - \frac{1}{\sqrt{1 + i_{f2}} - 1} \right]^{-1}. \quad (11)$$

In what follows, the LS and TC are computed using the box method, i.e.,

$$\text{LS} = \frac{(I_{REF,\max} - I_{REF,\min})}{I_{REF,\text{avg}}(V_{DD,\max} - V_{DD,\min})} \times 100 \% / \text{V}, \quad (12)$$

$$\text{TC} = \frac{(I_{REF,\max} - I_{REF,\min})}{I_{REF,\text{avg}}(T_{\max} - T_{\min})} \times 10^6 \text{ ppm}/^\circ\text{C}, \quad (13)$$

where $I_{REF,\min/\text{avg}/\max}$ respectively stand for the minimum, average, and maximum reference current among the considered range. $V_{DD,\min/\max}$ (resp. $T_{\min/\max}$) refer to the lower and upper bounds of the voltage (resp. temperature) range.

B. Operation Principle

In prior art [8], [9], a PTAT reference current is obtained with $V_{B6} = V_X$ and M_{6-7} sharing the same V_T type and length, thus yielding $\Delta V_T = 0$ and resulting in a purely PTAT voltage V_X [Fig. 3(a)]. Equation (8) subsequently becomes temperature-independent as the term in red amounts to zero. It also means that i_{f2} does not change with temperature

[Fig. 3(b)]. Ultimately, this forces I_{REF} to have the same temperature dependence as I_{SQ} , as stated by (9), and to follow a PTAT trend dictated by T^{2-m} [Fig. 3(c)].

In the proposed CWT current reference, an offset voltage $\Delta V_T > 0$ which is made CWT by design is added to V_X [Fig. 3(a)], augmenting (8) with the temperature-dependent term in red. This causes i_{f2} to decrease with temperature [Fig. 3(b)] and, with a proper selection of parameters ($K_{PTAT}; \alpha$), can make the temperature dependence of i_{f2} compensate that of I_{SQ} . This results in a temperature-independent I_{REF} as depicted in Fig. 3(c). An obvious question which arises at this stage is how to choose ($K_{PTAT}; \alpha$) to reach temperature independence. In Figs. 4(a) and (b), we study their impact on two figures of merit (FoMs) of the current reference, namely the TC of I_{REF} and $S_{I_{REF}}$, for a fixed CWT $\Delta V_T = 20$ mV, and generic technological parameters $n = 1.2$ and $m = 1.25$. Fig. 4(a) reveals the existence of an I_{REF} TC valley for a linear relationship between K_{PTAT} and α . Furthermore, this valley corresponds to an iso-sensitivity curve in Fig. 4(b). In Fig. 4(c), we assess the influence of ΔV_T on the location of the I_{REF} TC valley, and notice that increasing ΔV_T raises both the slope and offset of the linear relation between these two parameters. Technological parameters also have an influence on the valley location, with n and m having respectively an effect opposite and similar to ΔV_T . However, these parameters are fixed by the technology and we do not consider them as potential tuning knobs for design. Lastly, Fig. 4(d) depicts the evolution of the FoMs for ΔV_T ranging from 10 to 30 mV, $\alpha = 4$, and K_{PTAT} corresponding to the I_{REF} TC valley. It emphasizes that a constant 80-ppm/°C TC can be achieved with a proper choice of parameters, but that $S_{I_{REF}}$ improves from 7.33 to 2.45 %/mV with a growing ΔV_T . This trend is explained by the fact that an increase in V_X pushes M_{1-2} further into moderate inversion and decreases $S_{I_{REF}}$, at the cost of an increased area for the SCM and a larger minimum supply voltage. The values taken by parameters ($K_{PTAT}; \alpha$) are thus practically limited by such considerations during the sizing.

C. Practical Implementation of ΔV_T

The question that remains to be answered is how the offset voltage ΔV_T is practically achieved in the proposed current reference, knowing that it should ideally be CWT to ease the sizing, and that it does not need to be very large, as $S_{I_{REF}}$ improves less and less for large ΔV_T values [Fig. 4(d)]. In addition, a large ΔV_T also increases voltage $V_{GS1} = V_G$ in the SCM, resulting in a larger minimum supply voltage. A good trade-off is thus to have ΔV_T around 20 to 25 mV. Note that in what follows, we opt for an implementation based on a pMOS SCM as it limits the area overhead by using n wells instead of triple wells, and by leveraging the lower specific current of pMOS devices compared to nMOS ones. Three options are available to obtain a threshold voltage difference between two transistors: (i) different V_T types, (ii) the same V_T type but different lengths, and (iii) leveraging FBB to change the V_T of one out of two transistors sharing the same V_T type and length. Figs. 5(a) and (b) illustrate the variations of $|V_{T0}|$ for pMOS devices, respectively in TSMC 65-nm bulk [Fig. 5(a)] in which

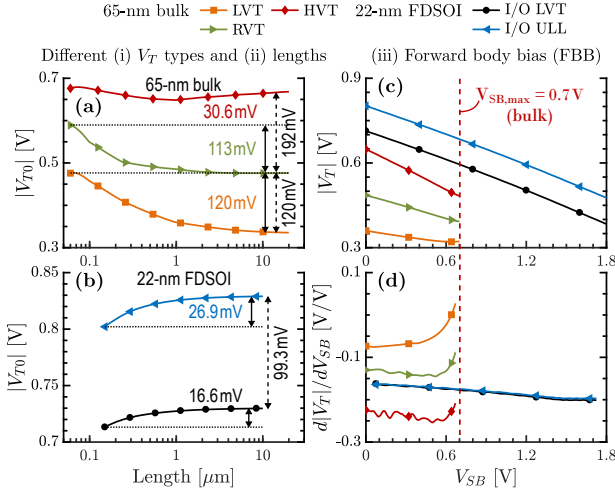


Fig. 5. All figures correspond to 1- μm -wide standard-well pMOS devices simulated at 25°C, and the threshold voltage is extracted from g_m/I_D vs. V_{SG} curves as described in [14]. $|V_{T0}|$ variations with the transistor length for (a) LVT, RVT and HVT core pMOS in 65-nm bulk and (b) LVT and ULL I/O pMOS in 22-nm FDSOI. For 1- μm -long devices, (c) $|V_T|$ and (d) $d|V_T|/dV_{SB}$ with V_{SB} for 65- and 22-nm devices. V_{SB} is limited by 0.7 V in 65 nm, to avoid the forward biasing of the parasitic diode between the transistor's source and body, and by the 1.8-V supply voltage in 22 nm.

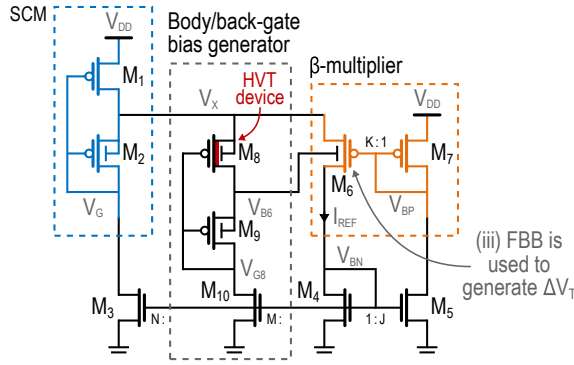


Fig. 6. Schematic of the proposed reference with a pMOS-based topology, featuring a low-power voltage reference to generate the body / back-gate voltage V_{B6} . This voltage reference is formed by transistors M_{8-10} and relies on the V_T difference between HVT and LVT pMOS in 65-nm bulk (resp. ULL and LVT pMOS in 22-nm FDSOI). Note that an nMOS-based topology is also possible, at the cost of a slightly larger silicon area due to the use of triple-well devices.

low-, regular- and high- V_T (LVT / RVT / HVT) core devices are available, and GF 22-nm FDSOI [Fig. 5(b)], in which low- V_T (LVT) and ultra-low-leakage (ULL) I/O devices are available. Both figures show that the V_T difference resulting from using different transistor types is typically between 0.1 and 0.2 V, and is hence much larger than the ΔV_T we seek to achieve. Then, the same V_T type but different lengths is a possibility to implement a ΔV_T in the desired range, with a difference from 31 to 120 mV in 65 nm, and from 17 to 27 mV in 22 nm. Nevertheless, this solution requires one of the transistors to be close to minimum length, which degrades other FoMs such as line sensitivity and mismatch, and leads to undesired second order effects due to the use of short-channel devices. Lastly, Figs. 5(c) and (d) represent the evolution of V_T and the derivative dV_T/dV_{SB} as a function of V_{SB} . Fig. 5(d) shows that in 65 nm, the body factor ranges from 74 to 244 mV/V depending on the V_T type, while in 22 nm, it is around 165 mV/V close to zero V_{SB} , i.e., body / back-gate

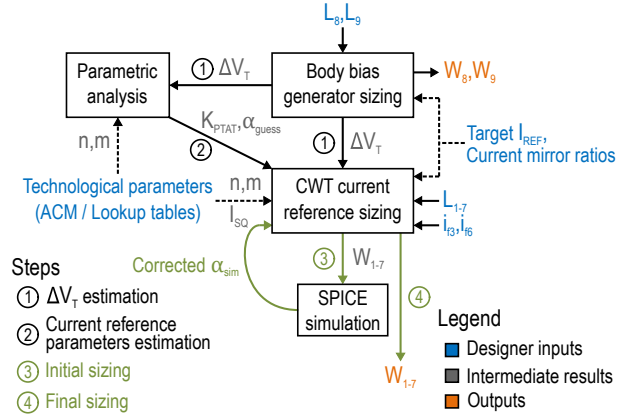


Fig. 7. Four-step flowchart of the design and sizing methodology.

and source connected to the same voltage. In this work, we choose to exploit FBB as it allows to obtain a positive offset ΔV_T contrary to RBB, provides a sufficient tuning range for a 20-to-25-mV ΔV_T , and offers the advantage of having devices M_{6-7} with the same technological parameters.

A schematic of the proposed current reference including the body / back-gate bias generator (M_{8-10}) is represented in Fig. 6. Note that the topology has been inverted compared to Fig. 2(a), i.e., nMOS and pMOS devices are swapped, as well as ground and supply voltage connections. The proposed reference is thus built around a pMOS-based SCM. The voltage reference is based on the ΔV_{SG} between an HVT (M_8) and LVT (M_9) devices biased by a current source (M_{10}). It generates a positive reference voltage thanks to the V_T difference between M_{8-9} , which are practically implemented with core HVT and LVT devices in 65 nm (resp. I/O ULL and LVT devices in 22 nm). Assuming a weak-inversion transistor in saturation, i.e., with $V_{SD} > 4U_T$, V_{SG} is expressed as

$$V_{SG} = |V_{T0}| + nU_T \log \left(\frac{I_{SD}}{I_{SQ}S} \right), \quad (14)$$

where $I_{SQ} = \mu C'_{ox}(n-1)U_T^2$ is another definition of the specific sheet current. Using (14), V_{SB6} is equal to

$$V_X - V_{B6} = |V_{T08} - V_{T09}| + nU_T \log \left(\frac{I_{SQ9}S_9}{I_{SQ8}S_8} \right), \quad (15)$$

in which the first term is either PTAT or complementary-to-absolute-temperature (CTAT) depending on the TC of the threshold voltages, and the second term's TC can be tuned by changing the ratio S_9/S_8 . This voltage reference will be sized so that ΔV_T between M_6 and M_7 is temperature-independent, as detailed in Section III-B. Finally, the voltage reference changes the ratio (3) to

$$\frac{S_1}{S_2} = \frac{I_{SQ2}}{I_{SQ1}} \frac{1 + M + N}{N} \frac{1}{\alpha - \beta}. \quad (16)$$

III. DESIGN AND SIZING METHODOLOGY

A. Overview of the Methodology

Fig. 7 provides a flowchart of the sizing methodology. It requires inputs from the designer, i.e., a target reference current, current mirror ratios, transistor lengths and inversion levels, as well as technological parameters, and it outputs transistor widths. The methodology is divided into four steps.

Step 1) consists in sizing the body/back-gate bias generator by selecting W_{8-9} such that ΔV_T 's TC is minimized.

Step 2) makes an educated guess of the value of α minimizing the TC of I_{REF} for a fixed K_{PTAT} , which is denoted as α_{guess} . The prediction is based on the linear relationship between K_{PTAT} and α obtained through the parametric analysis developed in Section II-A. It requires the ΔV_T computed by step 1), and technological parameters n and m , obtained by fitting the ACM model to g_m/I_D curves extracted from SPICE simulations as lookup tables [14].

Step 3) sizes the current reference for a range of α values and a fixed K_{PTAT} , based on ΔV_T and parameters n , m and I_{SQ} . Several sizings, which differ by the widths of M_{1-2} , are used to perform pre-layout SPICE simulations, from which we extract the value of α leading to a minimum I_{REF} TC. This value is referred to as α_{sim} and should be close to α_{guess} .

Step 4) simply consists in running the sizing algorithm with $\alpha = \alpha_{\text{sim}}$, thereby delivering the final transistor widths.

B. Body / Back-Gate Bias Generator

The setup employed to size the body / back-gate bias generator is illustrated in Fig. 8(a). It is composed of a low-power voltage reference formed by M_{8-9} , biased by an ideal current source $M \times I_{REF}$ with $M = 1$ and $I_{REF} = 1.25$ nA, and transistors M_{6-7} , respectively body-biased by a positive and zero V_{SB} . For M_{8-9} , we choose a relatively long length of $5 \mu\text{m}$ in 65 nm and $8 \mu\text{m}$ in 22 nm to reduce LS and variability. In Figs. 8(b) and (c), the width of M_{8-9} is swept from 0.5 to $5 \mu\text{m}$ in $0.1\text{-}\mu\text{m}$ steps to select the design point minimizing the TC of ΔV_T in 22 nm. Figs. 8(b) and (d) show that it corresponds to a slightly CTAT yet close to CWT $V_X - V_{B6}$, with a $123\text{-ppm}/^\circ\text{C}$ TC, and achieves a $31\text{-ppm}/^\circ\text{C}$ ΔV_T in Figs. 8(c) and (e). This result is consistent with the fact that ΔV_T is obtained through the back-gate effect, as described for an nMOS by $V_T(V_{BS}) = V_{T0} - \gamma_b V_{BS}$, where the body factor γ_b is temperature-independent at first order in FDSOI [15]. In 65 nm, a CTAT $1230\text{-ppm}/^\circ\text{C}$ $V_X - V_{B6}$ voltage is required to obtain a CWT $46\text{-ppm}/^\circ\text{C}$ ΔV_T , as it is obtained through the temperature-dependent body effect

$$V_T(V_{BS}) = V_{T0} + \gamma_b \left(\sqrt{2\phi_{fp} - V_{BS}} - \sqrt{2\phi_{fp}} \right), \quad (17)$$

where ϕ_{fp} is Fermi's potential.

C. Temperature-Independent Current Reference

The parametric analysis yields Figs. 9(a) and (b), which are akin to Fig. 4, but for 22 nm and a ΔV_T of 17.6 mV. As already described in Section II-B, the I_{REF} TC valley corresponds to a linear relationship between K_{PTAT} and α , along with an iso- $S_{I_{REF}}$ curve. Next, the current reference sizing per se can be performed in two ways. The first one is similar to the sizing methodology proposed in [8], [9] and is based solely on the ACM model. It consists of five main steps:

- Compute voltage V_X using (7);
- Solve (24) for i_{f2} , then calculate $i_{f1} = \alpha i_{f2}$, $S_{I_{REF}}$ from (11), and S_2 from (1);
- Solve (25) for β , calculate $i_{r1} = \beta i_{f2}$ and S_1 from (16);
- Compute the aspect ratio of M_{6-7} using (1);

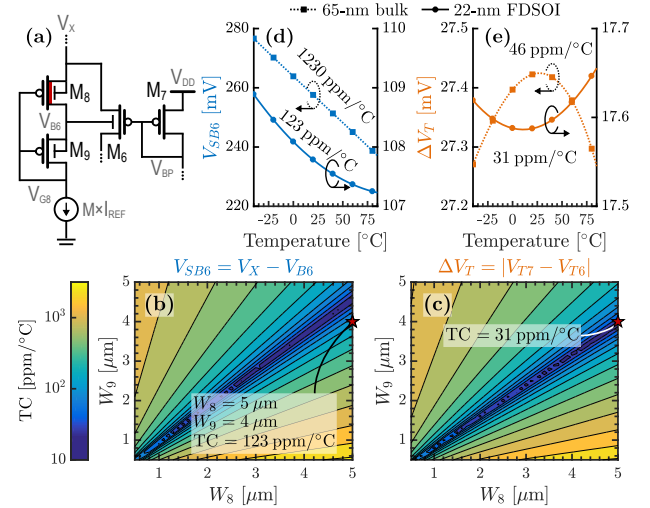


Fig. 8. ΔV_T is made CWT by tuning the TC of V_{SB6} by means of the ratio S_9/S_8 (15). All figures correspond to the behavior in TT. (a) Schematic and testbench of the low-power voltage reference used to generate V_{B6} . TC of (b) $V_X - V_{B6}$ and (c) ΔV_T , for different widths of M_{8-9} with $L = 8 \mu\text{m}$ in 22 nm. (d) Reference voltage $V_X - V_{B6}$ and (e) resulting threshold voltage difference ΔV_T as a function of temperature at the chosen design point.

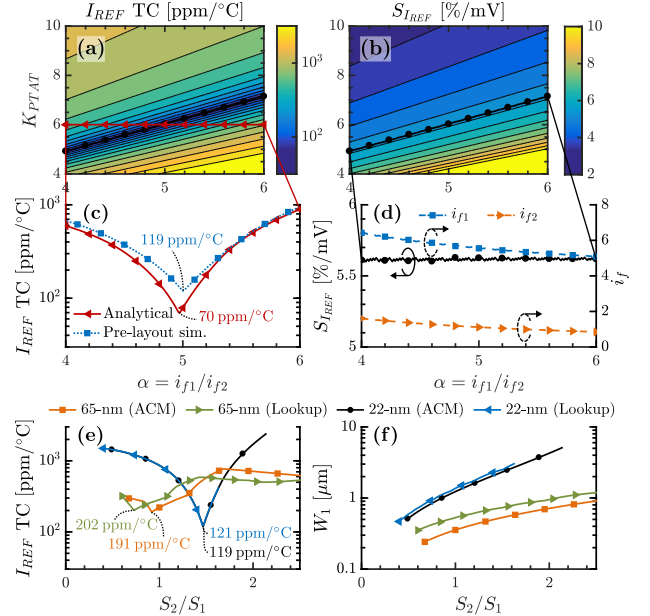


Fig. 9. I_{REF} is made CWT by properly selecting K_{PTAT} and α . (a) I_{REF} TC and (b) $S_{I_{REF}}$ for different values of (K_{PTAT} ; α) with $\Delta V_T = 17.6$ mV, $m = 1$, and $n = 1.2$, obtained from step 1) of the sizing methodology. In 22 nm and for different values of α , (c) I_{REF} TC computed from the analytical model and pre-layout simulation results, with the reference sized using an ACM-based approach, and (d) $S_{I_{REF}}$ and i_{f1} , i_{f2} . In 65 and 22 nm, (e) I_{REF} TC and (f) W_1 as a function of S_2/S_1 , for both ACM- and lookup-table-based sizings.

- Compute the aspect ratio of transistors M_{3-5} and M_{10} forming the current mirrors using (1).

The second way to perform the sizing replaces steps b) – c) by a direct use of lookup tables. The gate voltage of M_{1-2} is swept while keeping V_X to the value fixed by a), thus providing sizes complying with the SCM structure. This second method is theoretically more accurate, as transistors are better described by lookup tables than by a limited set of parameters.

Let us now take a closer look at the results of the sizing algorithm, with Figs. 9(a) to (d) presenting sizing results in

22 nm and Figs. 9(e) and (f), results in both 65 and 22 nm. Fig. 9(c) is obtained by fixing K_{PTAT} to 6 and extracting a slice of the 3D surface in Fig. 9(a). It reveals that the 70-ppm/ $^{\circ}\text{C}$ TC found for $\alpha_{\text{guess}} = 4.975$ closely matches the location of the minimum TC obtained from pre-layout simulations for $\alpha_{\text{sim}} = 5$, but differs in terms of value with a slightly larger 119-ppm/ $^{\circ}\text{C}$ TC. Moreover, Fig. 9(d) indicates that, along the I_{REF} TC valley, $S_{I_{REF}}$ remains stable around 5.62 %/mV while i_{f1} , i_{f2} decrease for larger values of α , as M_{1-2} are pushed closer to weak inversion. Then, Fig. 9(e) depicts the TC of I_{REF} computed from pre-layout simulations as a function of S_2/S_1 , which is a proxy for α (16). In 65 nm, pre-layout simulation results faintly diverge, with the ACM-based sizing leading to a 191-ppm/ $^{\circ}\text{C}$ TC at $S_2/S_1 = 0.92$, and the lookup-table-based one to a 202-ppm/ $^{\circ}\text{C}$ TC at $S_2/S_1 = 0.73$. In addition, the ACM-based sizing tends to output a narrower transistor M_1 than its lookup-table-based counterpart [Fig. 9(f)]. These discrepancies are presumably related to the approximated transistor behavior resulting from the estimation of ACM model parameters, as well as second order effects such as channel width modulation. In 22 nm, both sizing methods come up with a minimum at $S_2/S_1 = 1.47$, and Fig. 9(f) confirms that the sizes output by both algorithms are in close agreement.

IV. OPTIMIZATION AND SIMULATION RESULTS

This section comes in two parts. First, Sections IV-A and IV-B introduce architectural optimizations to the proposed reference, by respectively discussing how to improve LS and how to limit the TC degradation due to parasitic diode leakage at high temperature. Next, Section IV-C presents the schematic and post-layout simulation results of the proposed reference implemented in two common scaled technologies, i.e., TSMC 65-nm bulk and GF 22-nm FDSOI.

A. Line Sensitivity Improvement by Low-Voltage Cascoding

Low-voltage cascoding is often used in scaled technologies to improve LS without compromising the minimum supply voltage. An analytical approach allows to better grasp which transistors induce a dependence to supply voltage in the first place. The SCM in Fig. 6 can be simplified by a resistor [Fig. 10(a)] with an equivalent behavior around the operation point, denoted as Q . For this pMOS implementation, the resistance is given by

$$r_{SCM} = \left. \frac{\partial (V_{DD} - V_X)}{\partial I_{REF}} \right|_Q = \frac{1}{I_{REF} S_{I_{REF}}}. \quad (18)$$

Relying on the small signal schematic in Fig. 10(b) and first considering the case without transistor M_{6C} , i.e., $v_y = v_{bn}$, the absolute LS of V_X and the relative LS of I_{REF} around Q can be expressed as

$$\left. \frac{\partial (V_{DD} - V_X)}{\partial V_{DD}} \right|_Q = \frac{v_{dd} - v_x}{v_{dd}} = \frac{\frac{g_{d5}}{J} + g_{d6}}{g_{m6}}, \quad (19)$$

$$\left. \frac{1}{I_{REF}} \frac{\partial I_{REF}}{\partial V_{DD}} \right|_Q = \frac{1}{I_{REF}} \frac{i_{ref}}{v_{dd}} = S_{I_{REF}} \frac{v_{dd} - v_x}{v_{dd}}, \quad (20)$$

under the common assumption that $g_m \gg g_d = 1/r_o$. Equation (19) indicates that the dependence of $v_{dd} - v_x$ to v_{dd} can be attributed to M_{5-6} 's output conductance. Next, M_{6C} in

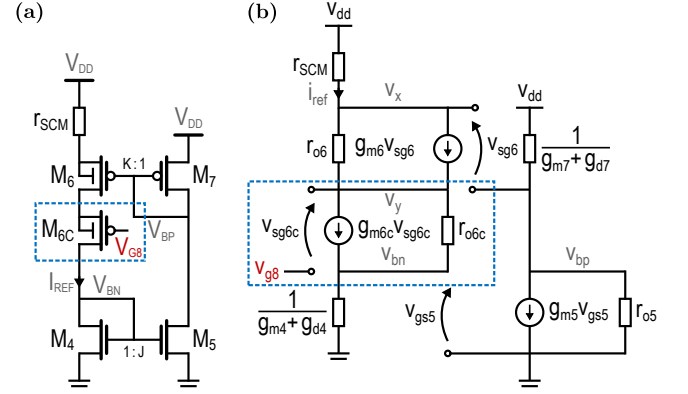


Fig. 10. (a) Schematic of the β -multiplier with low-voltage cascoding of M_6 through transistor M_{6C} . (b) Small signal schematic of (a).

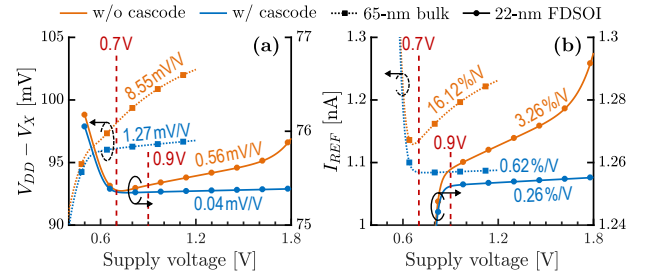


Fig. 11. Pre-layout simulations of (a) $V_{DD} - V_X$ and (b) I_{REF} with respect to the supply voltage in the TT 25 $^{\circ}\text{C}$ corner, highlighting the improvement of LS achieved by cascoding M_6 in both 65- and 22-nm technologies. The minimum supply voltage is 0.7 V in 65 nm and 0.9 V in 22 nm.

Fig. 10(a) is used to cascode M_6 , and is biased by voltage V_{G8} originating from the body / back-gate bias generator [Fig. 6]. A complete low-voltage cascode as depicted in Fig. 14(b) can also be used, but does not bring any significant LS improvement as M_7 is in diode and already has negligible V_{DS} variations. Based on Fig. 10(b) and assuming that $v_{g8} \approx v_x$, the absolute LS of V_X becomes

$$\frac{v_{dd} - v_x}{v_{dd}} = \frac{\frac{g_{d5}}{J}}{g_{m6} + \left(\frac{g_{d6}}{g_{m6C}} \right) r_{SCM}} \approx \frac{\frac{g_{d5}}{J}}{g_{m6}}, \quad (21)$$

while the relative LS of I_{REF} is still given by (20). LS is reduced because g_{d6} no longer appears in (21), which is highly beneficial as M_6 is in weak inversion while M_5 is closer to moderate inversion, meaning that M_6 is shorter than M_5 and therefore has a larger output conductance. In addition, current mirrors are implemented using composite transistors, i.e., the series connection of devices sharing the same V_G and V_B [16], further reducing the output conductance.

In 65 nm, simulations without cascoding exhibit an LS of V_X and I_{REF} [Fig. 11] respectively worth 8.55 mV/V and 16.12 %/V, computed from 0.7 to 1.2 V using the **box method**. Based on the small signal parameters extracted at the center of the supply voltage range, i.e., 0.95 V, (19) predicts an LS of V_X of 7.81 mV/V which compares fairly well to the 8.25-mV/V simulated value, computed with **first-order finite differences** around Q rather than with the box method. Equation (20) links the LS of I_{REF} to $v_{dd} - v_x / v_{dd}$, and yields a 21.33-%/V value diverging from the 15.75-%/V simulation, likely due to an overestimation of $S_{I_{REF}}$. With cascoding, the LS of V_X and I_{REF} improve to 1.27 mV/V and 0.62 %/V.

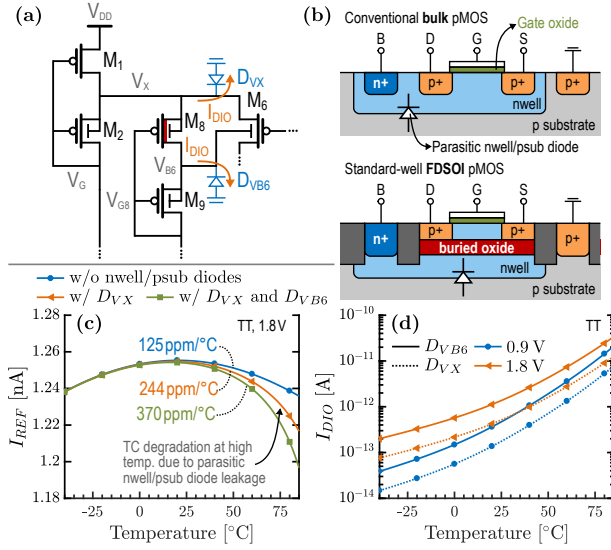


Fig. 12. I_{REF} TC is degraded by the leakage of parasitic nwell/psub diodes. (a) Schematic of the SCM and body / back-gate bias generator with parasitic diodes. (b) Cross-section of pMOS devices in conventional bulk and standard-well FDSOI technologies. (c) Temperature dependence of I_{REF} in TT 1.8 V, based on pre- and post-layout simulations in 22 nm. (d) Diode leakage as a function of temperature in 22 nm, for reverse voltages of 0.9 and 1.8 V.

Besides, the 0.90-mV/V LS of V_X prediction agrees with the 1.25-mV/V simulation. Similarly to the non-cascoded case, the 2.46-%/V prediction for the LS of I_{REF} is exaggerated compared to the 0.83-%/V simulation.

Simulations without cascoding in 22 nm yield a 0.56-mV/V LS of V_X and a 3.26-%/V LS of I_{REF} from 0.9 to 1.8 V. The small signal approach estimates an LS of V_X worth 0.35 mV/V around 1.35 V, which compares fairly well to the 0.33-mV/V simulated value. A 1.96-%/V LS of I_{REF} is predicted by (20) and closely matches the 1.89-%/V simulation, thus confirming the correct evaluation of $S_{I_{REF}} = 5.85$ %/mV. Cascoding reduces LS to 0.04 mV/V and 0.26 %/V for V_X and I_{REF} . Moreover, predictions give a 0.04-mV/V LS of V_X which agrees with the 0.038-mV/V simulation, while the LS of I_{REF} is accurately predicted to be 0.22 %/V, which is close to the 0.23-%/V simulation as for the case without cascoding.

To conclude, cascoding decisively diminishes I_{REF} LS by a factor 26× in 65 nm (resp. 12.5× in 22 nm) and comes for free in the proposed reference as V_{G8} is readily available from the body / back-gate bias generator.

B. Parasitic Diode Leakage Mitigation

In the case of a pMOS-based SCM [Fig. 12(a)] and at high temperature, I_{REF} TC is degraded by leakage currents flowing from V_X and V_{B6} to ground through parasitic nwell/psub diodes. The origin of these diodes is illustrated by the cross-section of pMOS devices in Fig. 12(b). This issue does not occur in 65 nm due to the lower reverse voltage applied to the diodes and the limited nwell area required by M_{6-6C-9} , as smaller devices can be used because of the low $S_{I_{REF}}$. Therefore, we only discuss the 22-nm design in what follows. Next, Fig. 12(c) shows that in 22 nm, the pre-layout simulation in TT 1.8 V features a 125-ppm/°C TC, while post-layout simulations with either diode D_{VX} or both diodes D_{VX} and D_{VB6} result in a degraded I_{REF} TC of 244 and 370 ppm/°C,

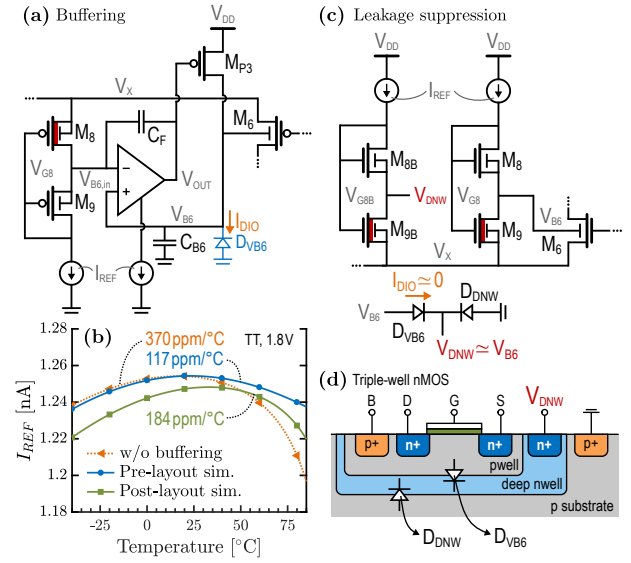


Fig. 13. Schematic of the body/back-gate bias generator (a) with a buffering stage implemented as an LDO, or (c) with a leakage suppression mechanism, obtained by implementing M_6 with a triple-well nMOS device whose deep nwell is biased by a body bias generator replica. (b) Temperature dependence of I_{REF} in pre- and post-layout simulations, with a fine-tuning of the SCM sizes in TT 1.8 V. (d) Cross-section of triple-well nMOS devices.

respectively. This degradation arises from the exponential increase of diode leakage with temperature [Fig. 12(d)], causing a deviation from the pre-layout behavior above 50°C. D_{VB6} 's leakage attains 21 to 33.8 pA at 85°C and mostly has an indirect impact on I_{REF} by inducing a change in V_{B6} , passed on I_{REF} through ΔV_T . Furthermore, D_{VX} 's leakage at 85°C lies between 7.8 and 12.5 pA and has a direct impact on I_{REF} by drawing some current away from the SCM and β -multiplier. However, it should be noted that this impact can be alleviated by connecting the body of M_2 to V_{DD} while accounting for this change in the sizing of the SCM.

In Fig. 13, two solutions are proposed to combat the adverse effect of parasitic diode leakage. First, a low-dropout (LDO) regulator copes with D_{VB6} 's leakage by buffering node $V_{B6,in}$ [Fig. 13(a)]. It consists of four main components: (i) a self-biased 4T operational transconductance amplifier (OTA) with an nMOS differential pair, (ii) a regulation pMOS M_{P3} delivering the leakage current of D_{VB6} , (iii) a capacitor C_{B6} ensuring the stability of the LDO, and (iv) a Miller capacitor C_F ensuring the stability of the whole reference by adding a dominant pole $f_{pd} = (g_{m8} + g_{d8}) / (2\pi C_F A_{v,OTA})$ at node $V_{B6,in}$, with $A_{v,OTA}$ the differential voltage gain of the OTA in DC conditions. Fig. 13(b) reveals that a 117-ppm/°C I_{REF} TC is obtained pre-layout with this additional buffering stage. With a fine-tuning of the SCM sizes to alleviate the impact of D_{VX} 's residual leakage, an increase of the TC to 184 ppm/°C is observed post-layout, albeit the degradation is lessened compared to the 370 ppm/°C without buffering. At last, the buffering stage entails power and area overheads corresponding to 14.3 % (0.83 nW) and 14.7 % (1940 μm^2) of the total power and area usage.

Second, in the case of an nMOS-based SCM, leakage suppression could be achieved by biasing the deep nwell with a voltage $V_{DNW} \approx V_{B6}$. This technique is inspired from ultra-low-power voltage references [17], and forces a

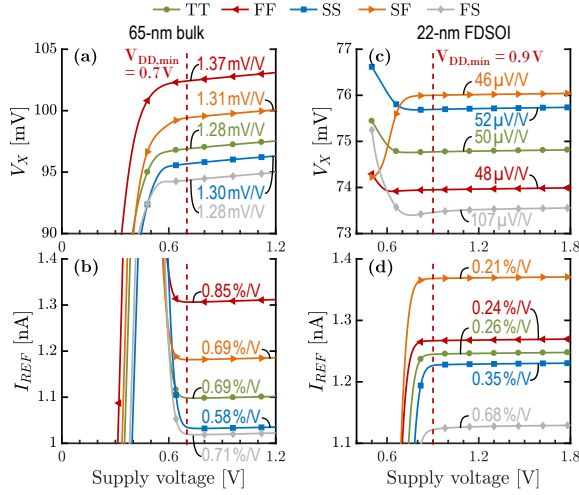


Fig. 16. Post-layout simulations of the supply voltage dependence of V_X and I_{REF} in all process corners and at 25°C, in 65-nm bulk [(a) and (b)] and in 22-nm FDSOI [(c) and (d)].

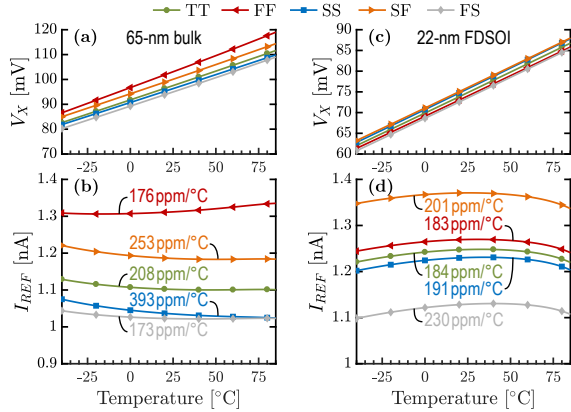


Fig. 17. Post-layout simulations of the temperature dependence of V_X and I_{REF} in all process corners, at 1.2 V in 65-nm bulk [(a) and (b)] and at 1.8 V in 22-nm FDSOI [(c) and (d)].

yields a 0.69-%/V LS of I_{REF} [Fig. 16(b)]. Process variations have negligible impact on the LS but change I_{REF} by +19.09 % in FF and -7.20 % in SF. Fig. 17(a) highlights the slightly different TC of V_X due to process variations of the subthreshold slope factor. These differences result in I_{REF} TC discrepancies, with a typical and worst-case values of 208 and 393 ppm/°C. Regarding variability, only mismatch can be simulated in 65 nm as no statistical models for global process variations are available in the process design kit (PDK) used in this work. Fig. 18(a) exhibits a 2.92-% (σ/μ) lower than the 3.74 % inferred from (23) and the 1.37-mV σ_{V_X} , concurring with the hypothesis of an $S_{I_{REF}}$ overestimation. Regarding TC, its median and 99th percentile are 213 and 431 ppm/°C [Figs. 18(b) and (c)]. Finally, the typical and worst-case startup times t_s are 3.4 and 29.2 ms [Fig. 19(a)].

In 22 nm, the layout [Fig. 15(b)] is dominated by M_{6-7} , which need to be large to minimize σ_{V_X} and thus account for 28.7 % of the 0.0132-mm² area. Then, regarding supply voltage dependence, the slender process variations impacting V_X [Fig. 16(c)] stem from V_{B6} through ΔV_T . However, I_{REF} is mainly impacted by I_{SQ} variations [Fig. 16(d)], and changes by at most +9.85 % in SF and -9.51 % in FS. From 0.9 to 1.8 V, the LS of V_X is worth 50 $\mu V/V$ in TT, and translates to a

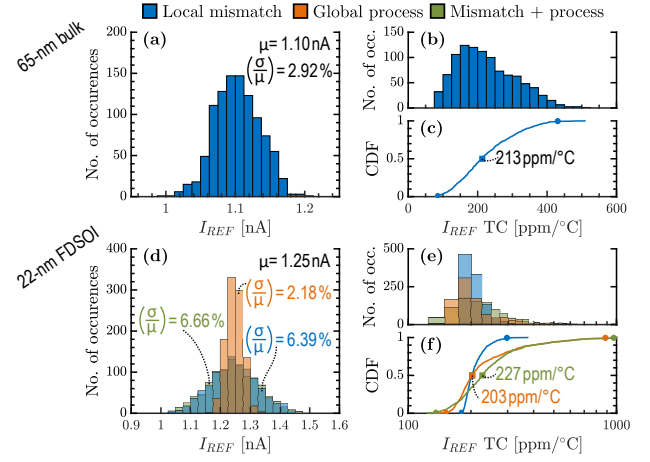


Fig. 18. For 10^3 post-layout MC simulations in TT, histograms of I_{REF} at 25°C, and I_{REF} TC from -40 to 85°C, at 1.2 V in 65-nm bulk [(a) to (c)] and 1.8 V in 22-nm FDSOI [(d) to (f)]. (d) to (f) correspond to simulations of local mismatch, global process variations, and their combined effects.

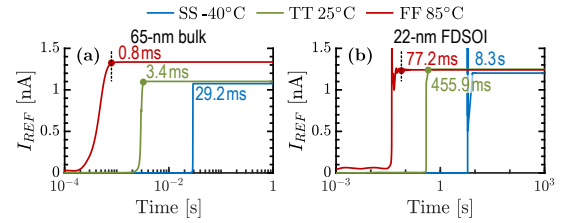


Fig. 19. Post-layout startup waveforms in the fastest (FF 85°C), typical (TT 25°C), and slowest (SS -40°C) corners, (a) at 1.2 V in 65-nm bulk and (b) 1.8 V in 22-nm FDSOI in the three process and temperature corners, using a voltage source with a rise time of 100 μs .

0.26-%/V LS of I_{REF} . Furthermore, LS is relatively constant across process corners except in FS, for which the 0.68-%/V value can be explained by the distortion close to 0.9 V. It requires a higher V_{DD} to cope with the increased pMOS V_T . Then, V_X has the same TC across process corners [Fig. 17(c)], leading to similar I_{REF} TCs in Fig. 17(d). The typical and worst-case TCs are 184 and 230 ppm/°C, the latter being partially explained by the lower I_{REF} value in this process corner, as I_{REF} TC is a relative metric. As far as variability is concerned, in 22 nm, we can simulate the impact of mismatch, process variations, and their combined effects. On the one hand, mismatch has a strong impact on I_{REF} (σ/μ) due to the large $S_{I_{REF}}$. The simulated 0.87-mV σ_{V_X} leads to a 4.92-% (σ/μ) prediction, which falls short of the 6.39-% simulation [Fig. 18(d)] due to additional mismatch in the SCM and the mirrors. Besides, TC variability is relatively limited, with a 203- and 299-ppm/°C median and 99th percentile [Figs. 18(e) and (f)]. On the other hand, process variations have a restricted impact on I_{REF} , with a 2.18-% (σ/μ), but deteriorate I_{REF} TC, with a 99th percentile shifted to 887 ppm/°C due to a malfunction of the buffer for extreme process realizations causing I_{REF} to drop at high temperature. Unsurprisingly, the combined effects yield a 6.66-% (σ/μ) for I_{REF} , together with a 227- and 972-ppm/°C median and 99th percentile for I_{REF} TC. Lastly, the typical and worst-case t_s are 456 ms and 8.3 s [Fig. 19(b)], because of the parasitic caps of large transistors. While the worst-case 8.3-s t_s could be critical, most applications require the reference to operate

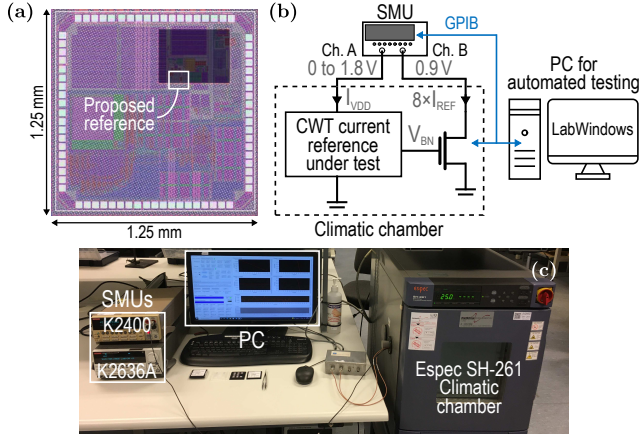


Fig. 20. (a) Chip microphotograph in GF 22-nm FDSOI, with the proposed reference highlighted in white. (b) Conceptual and (c) actual measurement testbench for supply voltage and temperature dependence characterization.

down to -40°C but not to start in the extreme SS -40°C corner, as nA-range current references are often always-on circuits. Nevertheless, this issue can be solved by widening M_{S2-S3} in Fig. 14(b), at the expense of a TC degradation in FF 85°C .

V. MEASUREMENT RESULTS

In this section, we describe the testbench used to characterize the proposed current reference, fabricated in GF 22-nm FDSOI as part of a 1.56-mm^2 microcontroller unit for biomedical applications codenamed ICare [Fig. 20(a)]. Then, we present the LS and TC measurements across the 20 dies in Figs. 21 and 22, before discussing the discrepancies with respect to post-layout simulations based on Figs. 23 and 24.

A. Measurement Testbench

Conceptual and actual views of the testbench are shown in Figs. 20(b) and (c). Supply voltage dependence is characterized using a two-channel Keithley K2636A source measurement unit (SMU), providing the supply voltage to the reference on channel A, and a 0.9-V V_{DS} to the output nMOS transistor on channel B. The supply current I_{VDD} and the output current, equal to $8 \times I_{REF}$, are measured by the K2636A, while a K2400 supplies the I/O voltage [Fig. 20(c)]. Supply voltage is then swept from 0 to 1.8 V in 25-mV steps. Then, temperature dependence is characterized using an Espec SH-261 climatic chamber which sweeps temperature from -40 to 85°C in 5°C steps. Both equipments are connected in GPIB to a PC running a testing routine in LabWindows. Lastly, LS and TC are computed across the 20 dies according to (12) and (13).

B. Supply Voltage and Temperature Dependence

Firstly, Fig. 21 quantifies the LS and variability of I_{REF} obtained in measurement at 25°C . Fig. 21(a) describes the supply voltage dependence of I_{REF} for post-layout simulations in TT and for the measurements average. The measured $V_{DD,min}$ remains about 0.9 V as expected from simulation, but I_{REF} shrinks from 1.25 to 0.9 nA. This difference cannot be explained by the mismatch of the mirror between I_{REF} and the output current, as the current ratio has a limited 1.5-% (σ/μ) evaluated from 10^3 MC simulations. As hypothesized

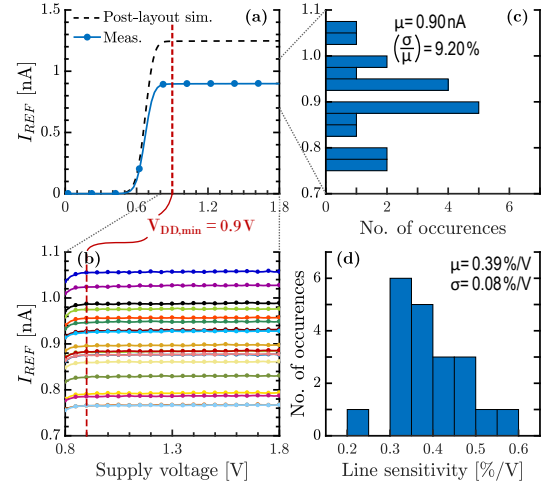


Fig. 21. (a) Post-layout-simulated and measured average I_{REF} , with (b) details of the 20 dies. Measured histograms of (c) I_{REF} at 1.8 V and (d) LS from 0.9 to 1.8 V. All figures are obtained at a temperature of 25°C .

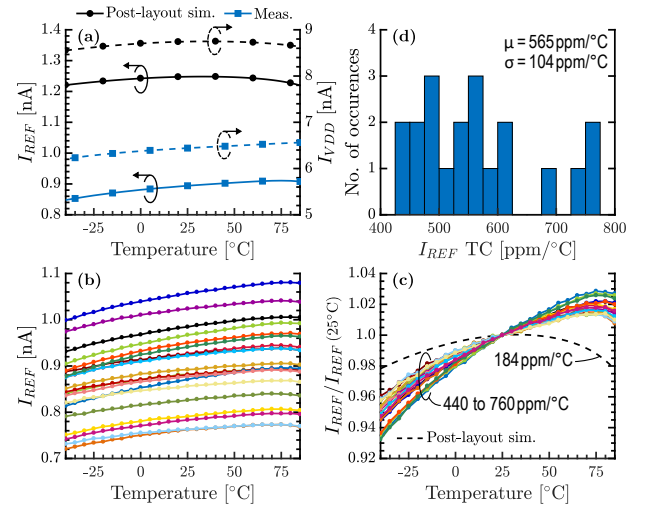


Fig. 22. (a) Post-layout-simulated and measured temperature dependence of the average I_{REF} and I_{VDD} . Measured temperature dependence of I_{REF} (b) without and (c) with normalization by the value at 25°C , for the 20 dies. (d) Measured histogram of I_{REF} TC from -40 to 85°C . All figures are obtained for a supply voltage of 1.8 V.

in [12] and confirmed in this work, this reduction is linked to global process variations and more specifically to skewed process corners of the ULL and LVT I/O devices M_8 and M_9 constituting the body / back-gate generator, as illustrated in Figs. 23(a) and 24(a). Details of the 20 dies are depicted in Fig. 21(b), and histograms of I_{REF} at 1.8 V and LS from 0.9 to 1.8 V are respectively presented in Figs. 21(c) and (d). Fig. 21(c) features a 9.20-% (σ/μ) larger than the 6.66-% value obtained in Section IV-C, which takes both mismatch and statistical process variations into account. Assuming the mean has been perfectly estimated, the 99-% confidence interval (CI) for the variance gives a CI for (σ/μ) equal to [7.3 %; 15.3 %], meaning that the limited sample size cannot explain the (σ/μ) discrepancy. The lower I_{REF} and higher (σ/μ) are rather explained by a CWT offset ΔV_T lower than its nominal value [Figs. 23(a) and (c)], the larger variability being linked to an increased sensitivity $S_{I_{REF}}$ as M_{1-2} 's inversion level is reduced. Finally, Fig. 21(d) reveals that

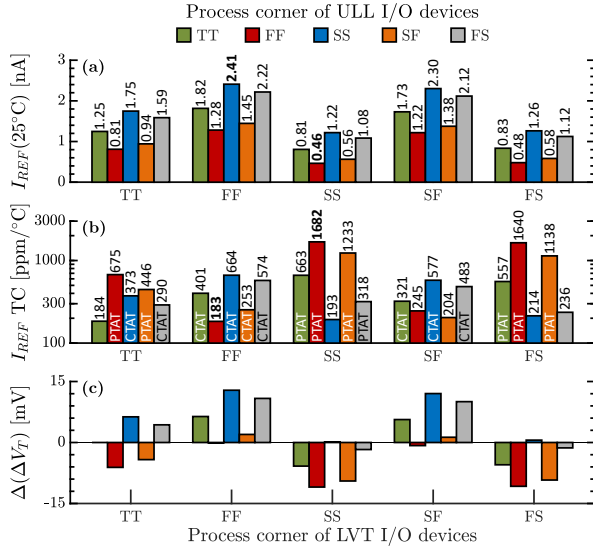


Fig. 23. Skewed process corners of ULL and LVT I/O devices have an impact on (a) I_{REF} at 25°C and (b) I_{REF} TC from -40 to 85°C , due to (c) changes in the CWT offset ΔV_T with respect to its nominal value. All results are obtained for a supply voltage of 1.8 V and a typical process for parasitic nwell/psub diodes.

the measured LS is around $0.39\text{ } \%/V$, which is close to the $0.26\text{ } \%/V$ obtained in post-layout simulation.

Furthermore, Fig. 22 gauges the temperature dependence of I_{VDD} and I_{REF} at 1.8 V . Fig. 22(a) highlights the second order behavior of I_{REF} in simulation and measurement, as well as a slightly PTAT trend observed in measurement only. I_{VDD} amounts to 8.8 nA in simulation (resp. 6.4 nA in measurement), leading to a 7.8-nW (resp. 5.8-nW) power consumption at 0.9 V . Details of the 20 dies are portrayed in absolute value in Fig. 22(b), and normalized by the value of I_{REF} at 25°C in Fig. 22(c). The measured TC is comprised between 440 and $760\text{ ppm}/^\circ\text{C}$, with an average of $565\text{ ppm}/^\circ\text{C}$ [Fig. 22(d)]. Skewed process variations of ULL and LVT I/O devices reliably explain the TC deterioration, as a decreased (resp. increased) ΔV_T compared to its nominal value results in a slightly PTAT (resp. CTAT) behavior [Figs. 23(b) and (c)]. Besides, Fig. 24 depicts the process corners showing the closest agreement with the measurements in terms of I_{REF} and TC, with TCs of 446 and $557\text{ ppm}/^\circ\text{C}$ observed in the (TT, SF, typ.) and (FS, TT, typ.) process corners, respectively [Fig. 24(a)]. These results much better coincide with the measured $565\text{-ppm}/^\circ\text{C}$ TC than the nominal corner [Fig. 24(b)]. Finally, Fig. 24 suggests that the measurements are better explained by a minimum process for the parasitic nwell/psub diode D_{VX} than by a typical process.

VI. COMPARISON TO THE STATE OF THE ART

This section compares our work to the state of the art of current references through some important trade-offs, illustrated in Fig. 25, and focuses on nA-range CWT references in Table II. We report post-layout simulation results in 65-nm bulk and 22-nm FDSOI, and measurement results in 22-nm FDSOI, corresponding to the three orange markers in Fig. 25. Firstly, the 65-nm design surpasses all references in Table II, simulated or fabricated, with a 0.0021-mm^2 area, and offers a $25\times$ reduction compared to prior art of fabricated references. Then, the

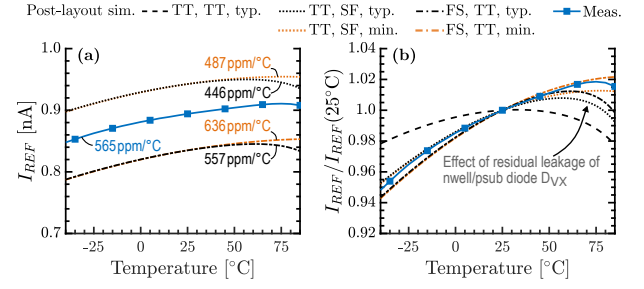


Fig. 24. Post-layout-simulated and measured temperature dependence of I_{REF} at 1.8 V (a) without and (b) with normalization by the value at 25°C . Post-layout simulations correspond to skewed process corners for LVT I/O devices, ULL I/O devices, and parasitic nwell/psub diodes.

0.0132-mm^2 silicon area in 22 nm outperforms all other fabricated references in Table II by at least a factor $4\times$, except for [24] whose $28.5\text{-}\mu\text{W}$ power consumption is prohibitive in most applications. Fig. 25(a) further demonstrates that the proposed references are almost unchallenged in terms of silicon area among nA-range CWT references, and lie beyond the trade-off of conventional references. Only [22] is competitive in terms of silicon area with a 0.0093-mm^2 design, as it relies on diode-connected and zero- V_{GS} transistors as voltage-to-current converter. However, it suffers from a strong degradation of other FoMs with a $2\text{-V } V_{DD,\text{min}}$, an $11\text{-}\%/V$ LS and a $20.3\text{-}\%$ (σ/μ). The low area overhead of the proposed reference is linked to the fact that it relies solely on transistors, contrary to other references which include area-hungry resistors. Besides, the implementation in advanced technology nodes further helps reducing the absolute area overhead. They reach the lowest reference current among CWT references at the exception of gate-leakage-based ones, which could be modified to reach a nA-range current but only at the cost of a $10^2\text{-to-}10^3\times$ larger area.

In Table II, power consumption and minimum supply voltage are on par with the state of the art, while LS is among the best for nA-range references with a sub- $1\text{-}\%/V$ value obtained by low-voltage cascoding for both implementations, and backed by a large intrinsic gain g_m/g_d in FDSOI [28]. Next, in terms of TC, the 213- and $203\text{-ppm}/^\circ\text{C}$ simulated values obtained for the proposed 65- and 22-nm designs are faintly larger than the TC of other fabricated references [Table II and Fig. 25(b)]. However, the design proposed in [6], [10] relies on a temperature exponent of carrier mobility close to two and cannot be ported to most technologies, whereas [6], [7], [26] are area-hungry due to the use of resistors and/or OTAs, and [27] due to the use of a current DAC and a low-TC reference. The TC degradation of the proposed 22-nm design to $565\text{ ppm}/^\circ\text{C}$ in measurement calls for a TC calibration mechanism, extensively used by fabricated references in Table II [6], [7], [26], [27], to retrieve quasi simulation-level performance. Possible implementations could for example tune the current ratio between M_5 and M_4 using a binary-weighted mirror [7] to change K_{PTAT} , or the number of transistors connected in series to implement M_1 [5] to change α . In Fig. 25(c), the proposed references fare quite well against prior art but can simply not compete against gate-leakage-based (resp. resistor-based) references in the pA (resp. μA) range. Finally, Fig. 25(d) demonstrates that the proposed designs are competitive with most existing references

TABLE II
COMPARISON TABLE OF TEMPERATURE-INDEPENDENT nA-RANGE CURRENT REFERENCES.

	Huang [10]	Far [19]	Kim [20]	Cordova [21]	Santamaria [22]	Aminzadeh [23]	Kayahan [24]	Dong [25]	Ji [26]	Wang [11]	Wang [6]	Huang [7]	Lee [27]	Lefebvre This work		
Publication Year	ISCAS 2010	ROPEC 2015	ISCAS 2016	ISCAS 2017	ISCAS 2019	AEU 2022	TCAS-I 2013	ESSCIRC 2017	ISSCC 2017	VLSI-DAT 2019	TCAS-I 2019	TCAS-II 2020	JSSC 2020	JSSC 2022		
Type of work	Sim.	Sim.	Sim.	Sim.	Sim.	Sim.	Silicon	Silicon	Silicon	Silicon	Silicon	Silicon	Silicon	Sim.	Sim.	Silicon
Number of samples	N/A	N/A	N/A	N/A	N/A	N/A	90	32*	10	10	16	10	10	N/A	N/A	20
Technology	0.18 μ m	0.18 μ m	0.13 μ m	0.18 μ m	0.18 μ m	0.18 μ m	0.35 μ m	0.18 μ m	0.18 μ m	0.18 μ m	0.18 μ m	0.18 μ m	0.18 μ m	65nm	22nm	FDSOI
I_{REF} [nA]	2.05	14	27	10.86	2.66	6.7	25	35.02	6.64	6.46	9.77	11.6	1	1.10	1.25	0.9
Power [nW]	5.1	150	N/A	30.5	26	51	28500	1.02	9.3	15.8	28	48.64	4.5/14 ^b	5.41	7.84	5.81
	@0.85V	@1V		@0.9V	@2V	@1.1V	@5V	@1.5V	@N/A	@0.85V	@0.7V	@0.8V	@1.5V	@0.7V	@0.9V	
Area [mm ²]	N/A	0.0102	N/A	0.01	0.0093	0.46	0.0053	0.0169	0.055	0.062	0.055	0.054	0.332	0.0021	0.0132	
Supply range [V]	0.85 – 2.2	1 – 3.3	1.2	0.9 – 1.8	2 – 3.3 ^o	1.1 – 1.8	5	1.5 – 2.5	1.3 – 1.8	0.85 – 2	0.7 – 1.2	0.8 – 2	1.5 – 2	0.7 – 1.2	0.9 – 1.8	
LS [%/V]	1.35	0.1	N/A	0.54	11^o	0.03	150	3	1.16	4.15	0.6	1.08	1.4	0.69	0.26	0.39^d
Temperature range [°C]	0 – 150	0 – 70	-30 – 150	-20 – 120	-40 – 125	-40 – 120	0 – 80	-40 – 120	0 – 110	-10 – 100	-40 – 125	-40 – 120	-20 – 80	-40 – 85	-40 – 85	
TC [ppm/°C]	91	20	327	108	182	40.33	128/250*	282	680/283 [†]	138[‡]	149.8	169	289/265 ^b	213	203	565 ^d
I_{REF} var. (process) [%]	7.5	N/A	3.7	15.8/11.6 [†]	N/A	N/A	8/1.22*	4.7	N/A	N/A	+11.7/-8.7 ^o +17.6/-10.3 ^d	N/A	+19.1/-7.2	+9.9/-9.5	N/A	
I_{REF} var. (mismatch) [%]	N/A	5.8	N/A	N/A	20.30	0.70	1.4 (sim.)	1.6	4.07/1.19*	3.33	1.6	4.3	1.26/0.25[†]	2.92	6.39	9.20
Trimming	No	No	No	Yes (6b)	No	No	No	No	Yes	No	Yes (5b)	Yes (6b)	Yes (27b)	No	No	No
Special components	No	No	Res.	ZVT	No	Res., BJT	No	Res., BJT	No	Res.	Res.,	Res.	No	No	No	No

* 16 dies for the TT process corner and 4 dies for each of the FF, SS, SF and FS process corners. * Simulated and measured values. † Before and after trimming.

‡ Best TC, the average one is not reported. ^o Estimated from figures. ^d Mean measured value across the 20 dies. ^b For 25 and 2.5 minutes between two calibrations.

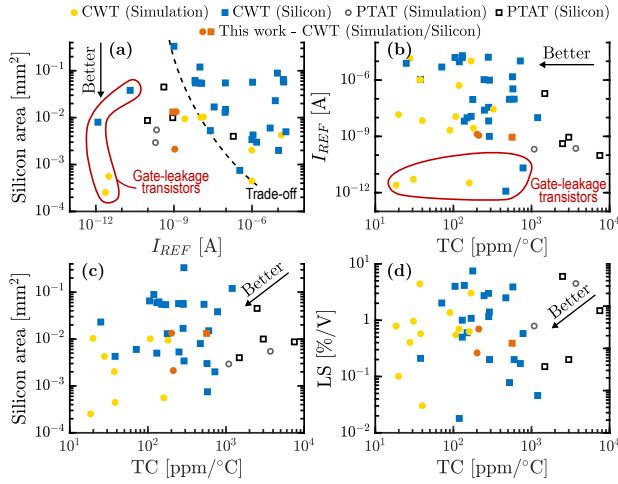


Fig. 25. Trade-offs between (a) area and I_{REF} , (b) I_{REF} and TC, (c) area and TC, and (d) LS and TC, based on the state of the art of current references.

in terms of LS and TC. The main drawback of the proposed 22-nm design is its large sensitivity to mismatch and process variations, with a 9.20-% (σ/μ) due to a large $S_{I_{REF}}$, which could be improved by increasing the sizes of M_{6-7} , or by increasing ΔV_T as it is done in the 65-nm design, whose simulated variability scales down to 2.92 %.

VII. CONCLUSION

In this work, we demonstrated a CWT current reference operating in the nA range. It relies on an SCM biased by a PTAT voltage with a CWT offset voltage, which stems from the V_T difference between transistors of the same V_T type, one of them being forward body-biased, through its body in bulk or back-gate in FDSOI. Then, we presented a comprehensive methodology for sizing the proposed reference based on the ACM model and validated it through post-layout simulations in 65-nm bulk and 22-nm FDSOI. The 65-nm reference produces a 1.1-nA current with an LS of 0.69 %/V and a TC of 213 ppm/°C, and power and area overheads of 5.4 nW and 0.0021 mm². Lastly, the 22-nm FDSOI design was fabricated and generates a 0.9-nA current with a 0.39-%/V LS and a 565-ppm/°C TC, while consuming 5.8 nW and occupying a silicon

area of 0.0132 mm². The TC degradation from simulation to measurement, together with the large 9.20-% variability due to mismatch and process variations, ask for a TC calibration scheme to be explored in further work.

APPENDIX A

ANALYTICAL EXPRESSIONS OF VOLTAGE V_X

Applying the ACM equations to transistors M_{1-2} forming the SCM [Fig. 2(b)] leads to two distinct equations. The first one is obtained by defining $\alpha \triangleq i_{f1}/i_{f2} > 1$ and expresses voltage V_X as

$$V_X = nU_T \left[\left(\sqrt{1 + \alpha i_{f2}} - \sqrt{1 + i_{f2}} \right) + \log \left(\frac{\sqrt{1 + \alpha i_{f2}} - 1}{\sqrt{1 + i_{f2}} - 1} \right) \right], \quad (24)$$

while the second one relates $\beta \triangleq i_{r1}/i_{f2} \in [0; 1]$ to voltage V_X and amounts to

$$V_X(n - 1) = nU_T \left[\left(\sqrt{1 + i_{f2}} - \sqrt{1 + \beta i_{f2}} \right) + \log \left(\frac{\sqrt{1 + i_{f2}} - 1}{\sqrt{1 + \beta i_{f2}} - 1} \right) \right]. \quad (25)$$

ACKNOWLEDGMENTS

The authors would like to thank Pierre Gérard for the measurement testbench, Eléonore Masarweh for the microphotograph, and ECS group members for their proofreading.

REFERENCES

- [1] L. Magnelli, F. A. Amoroso, F. Crupi, G. Cappuccino, and G. Iannaccone, "Design of a 75-nW, 0.5-V Subthreshold Complementary Metal-Oxide-Semiconductor Operational Amplifier," *Int. J. Circ. Theor. Appl.*, vol. 42, no. 9, pp. 967–977, Jan. 2013.
- [2] S. Jeong, I. Lee, D. Blaauw, and D. Sylvester, "A 5.8 nW CMOS Wake-Up Timer for Ultra-Low-Power Wireless Applications," *IEEE J. Solid-State Circuits*, vol. 50, no. 8, pp. 1754–1763, Apr. 2015.
- [3] H. Wang and P. P. Mercier, "A 14.5 pW, 31 ppm/°C Resistor-Less 5 pA Current Reference Employing a Self-Regulated Push-Pull Voltage Reference Generator," in *Proc. IEEE Int. Symp. Circuits Syst.*, 2016, pp. 1290–1293.

- [4] —, “A 3.4-pW 0.4-V 469.3ppm/°C Five-Transistor Current Reference Generator,” *IEEE Solid-State Circuits Lett.*, vol. 1, no. 5, pp. 122–125, May 2018.
- [5] H. Zhuang, J. Guo, C. Tong *et al.*, “A 8.2-pW 2.4-pA Current Reference Operating at 0.5V with No Amplifiers or Resistors,” *IEEE Trans. Circuits Syst. II, Exp. Briefs*, vol. 67, no. 7, pp. 1204–1208, July 2020.
- [6] L. Wang and C. Zhan, “A 0.7-V 28-nW CMOS Subthreshold Voltage and Current Reference in One Simple Circuit,” *IEEE Trans. Circuits Syst. I, Reg. Papers*, vol. 66, no. 9, pp. 3457–3466, Aug. 2019.
- [7] Q. Huang, C. Zhan, L. Wang *et al.*, “A -40 °C to 120 °C, 169 ppm/°C Nano-Ampere CMOS Current Reference,” *IEEE Trans. Circuits Syst. II, Exp. Briefs*, vol. 67, no. 9, pp. 1494–1498, Sept. 2020.
- [8] E. M. Camacho-Galeano, C. Galup-Montoro, and M. C. Schneider, “A 2-nW 1.1-V Self-Biased Current Reference in CMOS Technology,” *IEEE Trans. Circuits Syst. II, Exp. Briefs*, vol. 52, no. 2, pp. 61–65, Feb. 2005.
- [9] E. M. Camacho-Galeano, J. Q. Moreira, M. D. Pereira *et al.*, “Temperature Performance of Sub-1V Ultra-Low-Power Current Sources,” in *Proc. IEEE Int. Symp. Circuits Syst.*, 2008, pp. 2230–2233.
- [10] Z. Huang, Q. Luo, and Y. Inoue, “A CMOS Sub-1V Nanopower Current and Voltage Reference with Leakage Compensation,” in *Proc. IEEE Int. Symp. Circuits Syst.*, 2010, pp. 4069–4072.
- [11] J. Wang and H. Shinohara, “A CMOS 0.85-V 15.8-nW Current and Voltage Reference without Resistors,” in *2019 Int. Symp. VLSI Design Autom. Test*, 2019, pp. 1–4.
- [12] M. Lefebvre, D. Flandre, and D. Bol, “A 0.9-nA Temperature-Independent 565-ppm/°C Self-Biased Current Reference in 22-nm FD-SOI,” in *IEEE 48th Eur. Solid-State Circuits Conf.*, 2022, pp. 469–472.
- [13] A. I. A. Cunha, M. C. Schneider, and C. Galup-Montoro, “An MOS Transistor Model for Analog Circuit Design,” *IEEE J. Solid-State Circuits*, vol. 33, no. 10, pp. 1510–1519, Oct. 1998.
- [14] P. G. Jespers and B. Murmann, *Systematic Design of Analog CMOS Circuits*. Cambridge University Press, 2017.
- [15] E. M. da Silva, R. T. Doria, and R. T. Doria, “Effect of Substrate Bias and Temperature Variation in the Capacitive Coupling of SOI UTBB MOSFETs,” *J. Integr. Circuits Syst.*, vol. 16, no. 2, pp. 1–7, Aug. 2021.
- [16] C. Galup-Montoro, M. C. Schneider, and I. J. Loss, “Series-Parallel Association of FET’s for High Gain and High Frequency Applications,” *IEEE J. Solid-State Circuits*, vol. 29, no. 9, pp. 1094–1101, Sept. 1994.
- [17] L. Fassio, L. Lin, R. De Rose *et al.*, “Trimming-Less Voltage Reference for Highly Uncertain Harvesting Down to 0.25 V, 5.4 pW,” *IEEE J. Solid-State Circuits*, vol. 56, no. 10, pp. 3134–3144, May 2021.
- [18] S. Liu and R. J. Baker, “Process and Temperature Performance of a CMOS Beta-Multiplier Voltage Reference,” in *Proc. Midwest Symp. Circuits Syst.*, 1998, pp. 33–36.
- [19] A. Far, “Subthreshold Current Reference Suitable for Energy Harvesting: 20ppm/°C and 0.1%/V at 140nW,” in *2015 IEEE Int. Autumn Meet. Power Electron. Comput.*, 2015, pp. 1–4.
- [20] T. Kim, T. Briant, C. Han *et al.*, “A Nano-Ampere 2nd Order Temperature-Compensated CMOS Current Reference Using Only Single Resistor for Wide-Temperature Range Applications,” in *Proc. IEEE Int. Symp. Circuits Syst.*, 2016, pp. 510–513.
- [21] D. Cordova, A. C. de Oliveira, P. Toledo *et al.*, “A Sub-1 V, Nanopower, ZTC Based Zero-V_T Temperature-Compensated Current Reference,” in *Proc. IEEE Int. Symp. Circuits Syst.*, 2017, pp. 1–4.
- [22] J. Santamaria, N. Cuevas, L. E. Rueda G., J. Ardila, and E. Roa, “A Family of Compact Trim-Free CMOS Nano-Ampere Current References,” in *Proc. IEEE Int. Symp. Circuits Syst.*, 2019, pp. 1–4.
- [23] H. Aminzadeh and M. M. Valinezhad, “A Nano-Power Sub-Bandgap Voltage and Current Reference Topology with No Amplifier,” *AEU - Int. J. Electron. Commun.*, vol. 148, p. 154174, Mar. 2022.
- [24] H. Kayahan, Ö. Ceylan, M. Yazici *et al.*, “Wide Range, Process and Temperature Compensated Voltage Controlled Current Source,” *IEEE Trans. Circuits Syst. I, Reg. Papers*, vol. 60, no. 5, pp. 1345–1353, Mar. 2013.
- [25] Q. Dong, I. Lee, K. Yang *et al.*, “A 1.02 nW PMOS-Only, Trim-Free Current Reference with 282ppm/°C from -40°C to 120°C and 1.6% within-wafer inaccuracy,” in *IEEE 43rd Eur. Solid-State Circuits Conf.*, 2017, pp. 19–22.
- [26] Y. Ji, C. Jeon, H. Son *et al.*, “5.8 A 9.3 nW All-in-One Bandgap Voltage and Current Reference Circuit,” in *Proc. IEEE Int. Solid-State Circuits Conf.*, 2017, pp. 100–101.
- [27] S. Lee, S. Heinrich-Barna, K. Noh *et al.*, “A 1-nA 4.5-nW 289-ppm/°C Current Reference Using Automatic Calibration,” *IEEE J. Solid-State Circuits*, vol. 55, no. 9, pp. 2498–2512, Sept. 2020.
- [28] A. Cathelin, “Fully Depleted Silicon on Insulator Devices CMOS: The 28-nm Node Is the Perfect Technology for Analog, RF, mmW, and

Mixed-Signal System-on-Chip Integration,” *IEEE Solid-State Circuits Mag.*, vol. 9, no. 4, pp. 18–26, Nov. 2017.



Martin Lefebvre (Graduate Student Member, IEEE) received the M.Sc. degree (summa cum laude) in Electromechanical Engineering from the Université catholique de Louvain (UCLouvain), Louvain-la-Neuve, Belgium, in 2017, where he is currently pursuing the Ph.D. degree, under the supervision of Prof. D. Bol. His current research interests include hardware-aware machine learning algorithms, low-power mixed-signal vision chips for embedded image processing, and ultra-low-power current reference architectures. He serves as a reviewer for various conferences and journals, including IEEE Trans. on Biomed. Circuits and Syst., IEEE Trans. on VLSI Syst., Int. Symp. on Circuits and Syst. and Asia Pacific Conf. on Circuits and Syst.



Denis Flandre (Senior Member, IEEE) received the M.Sc. degree in Electrical Engineering, the Ph.D. degree and the Research Habilitation, from UCLouvain, Louvain-la-Neuve, Belgium, in 1986, 1990 and 1999, respectively. His doctoral research was on the modeling of silicon-on-insulator (SOI) MOS devices for characterization and circuit simulation, his post-doctoral thesis on a systematic and automated synthesis methodology for MOS analog circuits. Since 2001, he is full-time Professor at UCLouvain. He is involved in the research and development of SOI MOS devices, digital and analog circuits, as well as sensors, MEMS and solar cells, for special applications, more specifically ultra low-voltage low-power, microwave, biomedical, radiation-hardened and high-temperature electronics and microsystems. He has authored or co-authored more than 1000 technical papers or conference contributions. He is co-inventor of 12 patents. He has organized or lectured many short courses on SOI technology, devices and circuits in universities, industrial companies and conferences. He has received several scientific prizes and best paper awards. He has participated or coordinated numerous research projects funded by regional and European institutions. He has been a member of several EU Networks of Excellence on high-temperature electronics, SOI technology, nanoelectronics and micro-nano-technology. Prof. Flandre is a co-founder of CISSOID, a spin-off company of UCLouvain focusing on SOI and high-reliability integrated circuit design and products. He is scientific advisor of 3 other start-ups : INCIZE (semiconductor characterization and modeling for design of digital, analog/RF and harsh environment applications), e-peas (energy harvesting and processing solutions for longer battery life, increased robustness in all IoT applications) and VOCsSens (smart gas sensing solutions from edge to cloud).



David Bol (Senior Member, IEEE) is an Associate Professor at UCLouvain. He received the Ph.D. degree in Engineering Science from UCLouvain in 2008 in the field of ultra-low-power digital nanoelectronics. In 2005, he was a visiting Ph.D. student at the CNM, Sevilla, and in 2009, a post-doctoral researcher at intoPIX, Louvain-la-Neuve. In 2010, he was a visiting post-doctoral researcher at the UC Berkeley Lab for Manufacturing and Sustainability, Berkeley. In 2015, he participated to the creation of e-peas semiconductors spin-off company. Prof. Bol leads the Electronic Circuits and Systems (ECS) group focused on ultra-low-power design of integrated circuits for environmental and biomedical IoT applications including computing, power management, sensing and wireless communications. He is actively engaged in a social-ecological transition in the field of ICT research with a post-growth approach. Prof. Bol has authored more than 150 papers and conference contributions and holds three delivered patents. He (co-)received four Best Paper/Poster/Design Awards in IEEE conferences (ICCD 2008, SOI Conf. 2008, FTFC 2014, ISCAS 2020) and supervised the Ph.D. thesis of Charlotte Frenkel who received the 2021 Nokia Bell Scientific Award and the 2021 IBM Innovation Award for her Ph.D. He serves as a reviewer for various IEEE journals and conferences and presented several keynotes in international conferences. On the private side, Prof. Bol pioneered the parental leave for male professors in his faculty, to spend time connecting to nature with his family.